



A multiscale method for micro/nano flows of high aspect ratio

Matthew K. Borg^{a,*}, Duncan A. Lockerby^b, Jason M. Reese^a

^a Department of Mechanical and Aerospace Engineering, University of Strathclyde, Glasgow G1 1XJ, UK

^b School of Engineering, University of Warwick, Coventry CV4 7AL, UK

ARTICLE INFO

Article history:

Received 12 October 2011

Received in revised form 10 July 2012

Accepted 4 September 2012

Available online 20 September 2012

Keywords:

Multiscale simulations

Hybrid method

Molecular dynamics

Coupled solvers

Scale-separation

ABSTRACT

We develop a new multiscale scheme for simulating micro/nano flows of high aspect ratio in the flow direction, e.g. within long ducts, tubes, or channels, of varying section. The scheme couples conventional hydrodynamic conservation equations for mass and momentum-flux with molecular dynamics (MD) in a unified framework. The method is very much different from common ‘domain-decomposition’ hybrid methods, and is more related to micro-resolution methods, such as the Heterogeneous Multiscale Method. We optimise the use of the computationally-costly MD solvers by applying them only at a limited number of streamwise-distributed cross-sections of the macroscale geometry. The greater the streamwise scale of the geometry, the more significant is the computational speed-up when compared to a full MD simulation. We test our new multiscale method on the case of a converging/diverging nanochannel conveying a simple Lennard-Jones liquid. We validate the results from our simulations by comparing them to a full MD simulation of the same test case.

© 2012 Elsevier Inc. All rights reserved.

1. Introduction

There are many important and emerging micro and nano engineering applications that involve internal fluid flow: lab-on-a-chip devices, nanotube membranes for water purification [1] or for removal of CO₂ from air [2], micro/nano tribology problems [3], and miniaturised heat exchangers for cooling electric circuits.

From a fluid simulation perspective, what these engineering applications have in common is that a wide range of scales need to be resolved. The smallest scale is dictated by the smallest dimension of the channel, duct or pipe of interest, i.e. on the micro or nano scale. On the other hand, in engineering devices (e.g. membranes, fluidic networks, heat-exchangers, and bearings) their *length* in the flow or streamwise direction is likely to be several orders of magnitude larger, and not necessarily of a trivial geometry (i.e. not straight and of uniform section). This presents a serious simulation difficulty. On the one hand, such small cross-sectioned channels and tubes require a computationally-expensive modelling tool in order to predict the correct flow properties, such as shear stresses and mass flow rates; on the other hand, such tools are far too computationally intensive to apply to the entire geometry. What is needed is a multiscale modelling approach.

The past decade has seen a rapid increase in multiscale approaches to gas [4] and liquid flows [5]. Typically, these multiscale approaches combine different modelling methodologies, and so are referred to as *hybrids*. The general notion of these hybrids is to couple diverse macro and micro descriptions to model phenomena across disparate length and time scales, and at the fastest computational speed. In most liquid flow cases, the micro solver is chosen to be molecular dynamics (MD). Although accurate in its macroscopic predictions, provided the correct molecular interactions are chosen, MD is computationally very much restricted to the smallest systems and shortest time-scales, i.e. at the nano scale. Continuum

* Corresponding author. Tel.: +44 (0) 141 548 3131; fax: +44 (0) 141 552 5105.

E-mail addresses: matthew.borg@strath.ac.uk (M.K. Borg), duncan.lockerby@warwick.ac.uk (D.A. Lockerby), jason.reese@strath.ac.uk (J.M. Reese).

hydrodynamics, such as the well-known Navier–Stokes–Fourier (NSF) model, is still valid in most Newtonian flows even at the nano scale, provided the correct transport properties are chosen [6]. However, the NSF equations are invalid when the flow is either non-Newtonian (unknown constitutive relations), or dominated by surface effects (e.g. velocity slip in nano-channels), or in thermodynamic non-equilibrium (in the presence of high flow gradients, for example). The “best of both worlds” can be obtained by applying MD in regions of the flow where continuum hydrodynamics is inaccurate, and continuum hydrodynamics wherever MD is prohibitively expensive.

Two main techniques have evolved in the literature: (a) domain-decomposition methods (see, e.g. [7–9]) and (b) Heterogeneous Multiscale Methods (see, e.g. [10–12]). The natural and most common approach to a hybrid methodology is to observe that for Newtonian liquids the NSF equations lack physical accuracy only next to surfaces or interfaces. Domain-decomposition techniques recognise this, as illustrated in Fig. 1(a), by applying a micro solver at the surface and adjacent liquid, and applying a macro description in the bulk part of the flow. Although the domain is uniquely divided into separate micro and macro sub-domains, there is always an overlap present at their interface for mutual coupling of fluid information. Many strategies for coupling have been developed in the literature: matching state properties [13,14] for modelling steady-state or start-up flows (e.g. coupling through streaming velocity), conservative fluxes [15,16] for modelling transient flows (mainly mass, momentum and energy), or a mixture of both [17,18].

Domain-decomposition has its drawbacks: there is the challenging requirement for non-periodic boundary conditions (for MD) at the coupling interface, which is not a well-developed area. A more fundamental obstacle relating to the internal-flow geometries discussed above, is that there is no obvious way to decompose the domain into ‘near wall’ and ‘bulk’

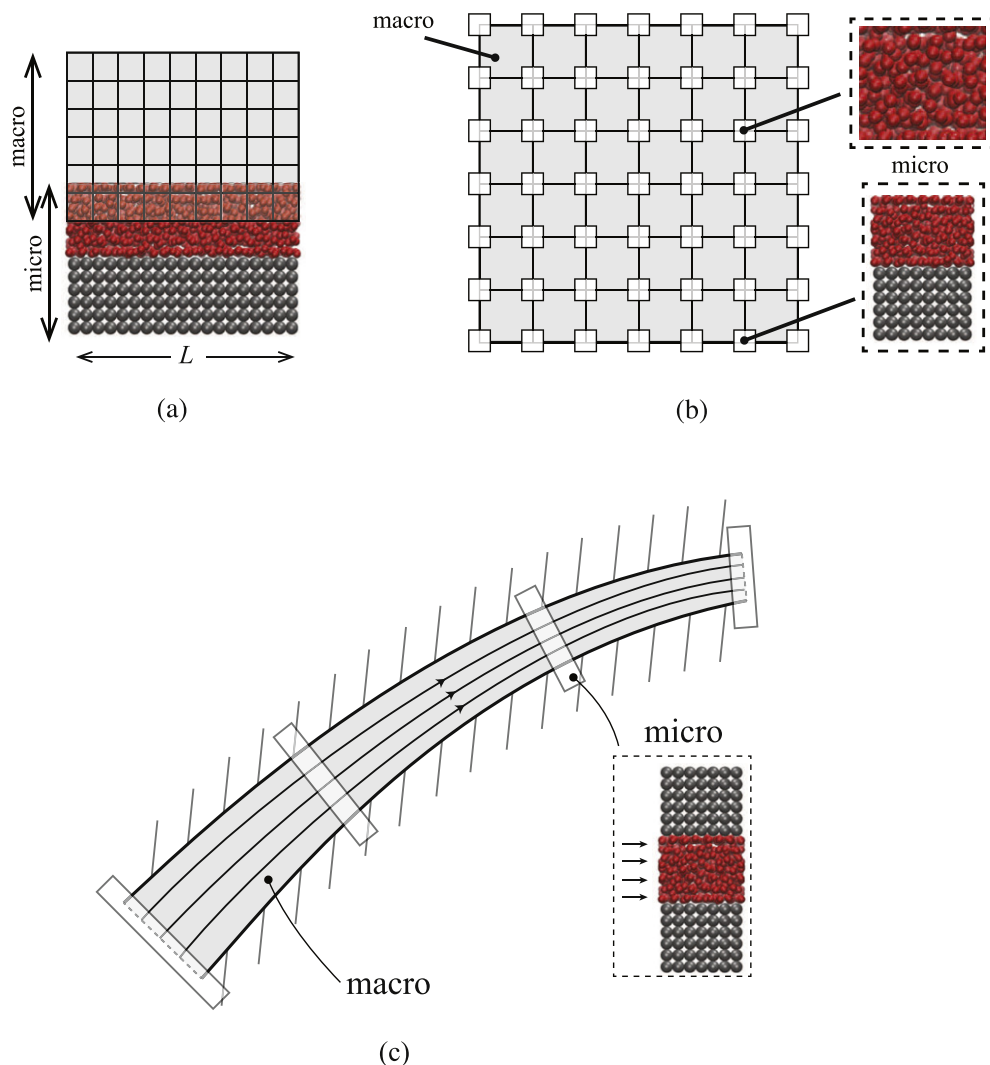


Fig. 1. Schematics of (a) the domain-decomposition method, (b) the Heterogeneous Multiscale Method (HMM), and (c) the multiscale method proposed in this paper.

regions when the *entire* flow in a micro or nano-channel geometry could be considered ‘near wall’. Even if a bulk region can be identified, the saving of domain-decomposition in such geometries is limited to the ratio of the bulk volume to the near-wall region volume. This is illustrated with reference to Fig. 1(a): to simulate larger L (a longer channel, say), the size of the micro sub-domain must be relatively increased, increasing the computational cost proportionally.

Less common multiscale techniques are the Heterogeneous Multiscale Method (HMM) [10–12], and its further development for time-scale separated problems, the seamless HMM [19]. In this type of multiscale, the objective is to employ *micro resolution* rather than micro–macro decomposition. In other words, the domain is entirely described by the macro model, with small isolated micro models spatially distributed in the domain, as shown in Fig. 1(b), that provide missing information to the macro solution locally. There are two scenarios where micro resolution is required. Like domain-decomposition methods, micro resolution is required in regions close to bounding surfaces. Micro elements in these regions are constrained from the continuum strain-rate field, and in turn provide an accurate local velocity slip and stress at the wall. As illustrated in Fig. 1(b), issues related to non-periodic boundary conditions still remain. The second scenario is for rheological fluids where the constitutive relations are unknown in the bulk of the flow, and micro resolution is therefore required over the entire flow domain to provide the unknown stress tensor field. The latter micro approach typically uses distributed MD boxes, as in Fig. 1(b), with modified periodic boundary conditions that deform the boxes to conform with the local velocity strain-rate: for example, the well-known Lees and Edwards shear boundary conditions [20].

The new multiscale method we propose in this paper is illustrated in Fig. 1(c). We focus on internal-flow problems in this paper, although the method could also be applied more generally to flows of high aspect ratio (in the streamwise direction) such as very thin coating flows, provided that the upper (in the case of coating flows, free surface) boundary conditions are properly represented. In all these problems, there is a gradual variation of hydrodynamic variables in the streamwise direction (so scale-separation can be exploited), whereas perpendicular to the flow no scale separation exists between the micro and macro processes.

The method we present to tackle this class of problem is related to the micro resolution (HMM) approach, with two major differences. First, in contrast to HMM techniques in the literature that attempt to impose velocity fields or strain-rates on micro simulations and then measure consequent stress, here we find it much more convenient and accurate to prescribe an emulated pressure-gradient to the micro simulations and measure streaming velocity or mass flux from the micro model in return. Second, our method avoids prescribing non-periodic boundary conditions or complex deformations on the MD box; instead we are able to use simple periodicity in all our micro sub-domains, making our approach more efficient as well as far more convenient.

Our method consists of applying a simple hydrodynamic description over the entire domain, and allocating micro sub-domains in very small ‘slices’ of the channel. Every micro element is an MD simulation (or other appropriate model, e.g. a direct simulation Monte Carlo method for micro-channel gas flows) over the local height of the channel, as shown in Fig. 1(c). The number of micro elements as well as their streamwise position is chosen to resolve the geometrical features of the macro channel. While there is no direct communication between individual micro elements, coupling occurs via an iterative imposition of mass and momentum-flux conservation on the macro scale. The micro elements replace the need to supply slip boundary conditions or stress–strain relationships to the hydrodynamic description: this is a major simplification to other hybrid methods.

The paper is organised as follows. In Section 2 we present in a general form our multiscale method, termed in this paper and for internal flow applications the “Internal-Flow Multiscale Method” (IMM). In Section 3, this approach is demonstrated on an axially-periodic converging–diverging nano-channel geometry. In Section 4 we present and compare simulation results from the IMM with results from a full MD simulation of the same case. Finally, conclusions are drawn in Section 5.

2. The Internal-flow Multiscale Method (IMM)

In the internal multiscale approach we describe here, individual micro sub-domains, covering the full cross-section of the channel or tube, are distributed in the streamwise direction with a spacing sufficient to resolve any streamwise variation in the channel/tube geometry. The key assumption in our method—and in fact what it is designed to exploit—is that there is a degree of scale separation between hydrodynamic variation along streamlines (i.e. in the s -direction, see Fig. 2(a)) and microscopic processes transverse to the flow direction (in y and z). For this scale separation to exist, the section geometry must vary slowly in the streamwise direction. A dimensionless number indicating the degree of such scale separation can be developed:

$$S = \min \left\{ \left| \frac{dL_y}{ds} \right|^{-1}, \left| \frac{dL_z}{ds} \right|^{-1}, \left| \frac{R_y}{L_y} \right|, \left| \frac{R_z}{L_z} \right| \right\}, \quad (1)$$

where L_y and L_z are length scales in perpendicular directions that characterise the cross-section geometry, and R_y and R_z are the radii of curvature of the centreline. Provided $S \gg 1$, we can safely assume that, in small streamwise sections of the tube/channel, the walls are approximately parallel to the centreline streamline (and consequently all other local streamlines). This we refer to as a *local parallel-flow assumption*, and it allows us to represent small sections of the channel/tube geometry by micro sub-domains with exactly parallel walls, as illustrated in Fig. 2(b).

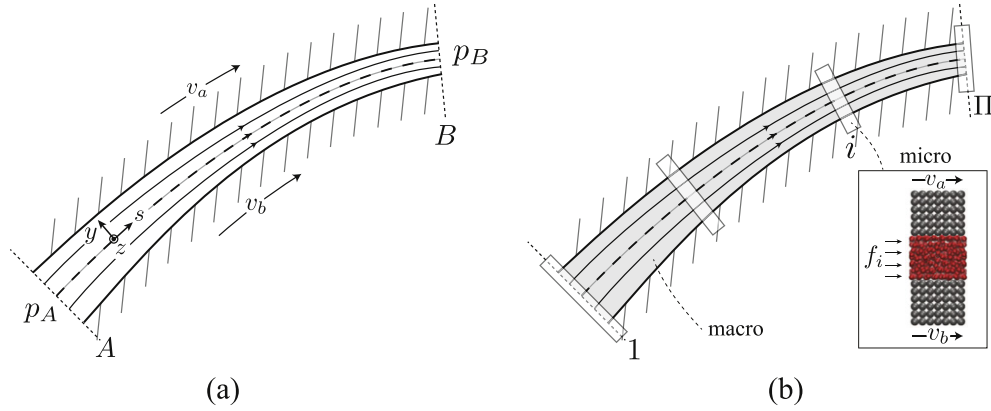


Fig. 2. Schematics of (a) a generic internal-flow configuration with non-stationary walls and imposed pressure difference and (b) domain partitioning in the Internal Multiscale Method, where f_i is a body force applied to the i th micro simulation.

The objective of our method is for the flow conditions in these otherwise independent micro sub-domains to represent the conditions that would be occurring at the same point in the whole flow geometry, i.e. in the macro domain. To do this a coupling needs to occur between the micro sub-domains and a valid macroscopic representation of the flow field.

2.1. The hydrodynamic conservation equations

We restrict our attention here to low-speed (low Reynolds number, low Mach number), steady-state flows, as these are of primary importance in the majority of applications discussed in the Introduction. In such conditions the equation for conservation of momentum for the generic channel/tube configuration of Fig. 2(a) is, in coordinates aligned with the local flow direction (with a local parallel-flow assumption):

$$\frac{\partial p}{\partial s} = \frac{\partial \tau_{sy}}{\partial y} + \frac{\partial \tau_{sz}}{\partial z} + F_s, \quad (2)$$

where τ_{sy} and τ_{sz} are perpendicular components of shear stress, p is the hydrostatic pressure, and F_s is a body force per unit volume in the flow direction.

For individual *decoupled* micro sub-domains (i.e. which do not involve, as yet, any macro connection) a different momentum balance is formed:

$$0 = \frac{\partial \tau_{sy}}{\partial y} + \frac{\partial \tau_{sz}}{\partial z} + F_s. \quad (3)$$

The difference between Eqs. (2) and (3) is the existence of a local pressure-gradient term, which in the macro domain is generated by a combination of the applied pressure difference ($p_B - p_A$, in Fig. 2(a)), and the requirement for mass continuity through the entire geometry. To facilitate a coupling mechanism between the micro and macro domains, the missing pressure gradient can be emulated within the micro subdomain by a fictitious body force, Φ , which we refer to as a *pressure-gradient correction*¹:

$$\Phi = \frac{\partial \tau_{sy}}{\partial y} + \frac{\partial \tau_{sz}}{\partial z} + F_s. \quad (4)$$

Provided the difference in pressure over the streamwise length of a micro domain is relatively small, the pressure-gradient correction force, Φ , is hydrodynamically equivalent to the effects of the missing pressure gradient, i.e.

$$\Phi \equiv \frac{\partial p}{\partial s}. \quad (5)$$

Note, because of our locally-parallel flow assumption, the pressure gradient (and consequently Φ) is constant across the cross-section.

The aim of the coupling methodology presented here is to find (by iteration) values of Φ for each micro subdomain which collectively ensure that: (a) the boundary conditions on pressure are correctly imposed ($p_B - p_A$) and (b) mass conservation is satisfied, i.e. the same mass flow rate is generated in each of the micro simulations.

¹ For certain types of micro solver the pressure gradient might be easy to impose directly without the need for a body force representation.

2.1.1. Satisfying the pressure-drop boundary condition

Eq. (5) can be integrated over the streamwise length of the channel/tube geometry to obtain:

$$\int_A^B \Phi \, ds = \Delta p, \quad (6)$$

where $\Delta p = p_B - p_A$. A numerical approximation to the continuous integral in Eq. (6) provides us with a constraint on values of Φ :

$$\sum_{i=1}^{\Pi} a_i \Phi_i \approx \Delta p, \quad (7)$$

where i denotes the i th of Π micro sub-domains (see Fig. 2(b)) and a_i are coefficients of an appropriate numerical quadrature (e.g. Simpson's rule). This alone, though, is not sufficient to constrain the Π individual values of Φ_i .

2.1.2. Satisfying the requirement for mass conservation

The requirement for mass conservation is satisfied if the mass flow rates in each of the micro sub-domains are equal. Each of the micro sub-domains can have a different cross-sectional geometry, and therefore to achieve a conserved mass flux, the pressure-gradient correction, Φ_i , will be different in each.

As a first guess in an iterative approach, we take the pressure gradient to be constant throughout the channel (i.e. $\Phi_i = \Delta p / L_s$ for all i , where L_s is the channel length). As a result, the individual micro solutions will generate mass flow rates that are not equal; some will be larger than the mean, and some will be lower. For those that are larger, the pressure-gradient correction force can be increased in some proportion to the deficit; for those that are lower than the mean, the correctional force can be reduced. Provided Eq. (7) is satisfied at each step, this process continues iteratively until both mass and momentum flux are conserved in the macro domain. Just for the purposes of improving the rate of convergence, we assume a proportional relationship between total applied body force ($F_s - \Phi_i$) and mass flow rate in a subdomain (\dot{m}_i) when making estimations for the pressure-gradient correction at the next iteration, Φ_i^* , which is based on a mass-flow-rate target common to all micro subdomains, \bar{m} , i.e.

$$\frac{F_s - \Phi_i^*}{\bar{m}} = \frac{F_s - \Phi_i}{\dot{m}_i},$$

which rearranges to:

$$\Phi_i^* = F_s + (\Phi_i - F_s) \frac{\bar{m}}{\dot{m}_i}. \quad (8)$$

Provided there is a monotonic relationship between $(F_s - \Phi_i)$ and \dot{m} this is a valid and efficient means of approaching a converged solution. A more detailed example of this iteration procedure is provided in the next section.

Solving a micro model (e.g. MD) for the Π sub-domains, with cross-sections corresponding to the macro geometry at those points, but with pressure-gradient corrections constrained by (7) and iteratively refined using (8), ensures conservation of both mass and momentum flux for the entire macroscopic geometry. This is the essence of what we term the Internal-flow Multiscale Method (IMM).

3. Application example: converging-diverging nano-channel flow

We demonstrate our method on an axially-periodic converging/diverging nano-channel flow that is driven by an external gravity-type force $f^{\text{ext}} = 0.487$ pN. Fig. 3 shows the flow geometry. The channel has dimensions: $L_x = 81.6$ nm; $h_{\text{inlet}} = 3.4$ nm and $h_{\text{throat}} = 2$ nm, while the geometry is periodic in the z direction, representing a 2D channel. For this geometry the scale-separation number defined in Eq. (1) is $S = 22.5$, which corresponds to streamlines that vary from the centre streamline (the dashed line in Fig. 3) by a maximum of 1.27 degrees. Our locally-parallel flow assumption, then, is a safe one.

The Reynolds number and Mach number for this case, based on average velocity through the throat, are $\text{Re} = 0.8$ and $\text{Ma} = 0.015$.

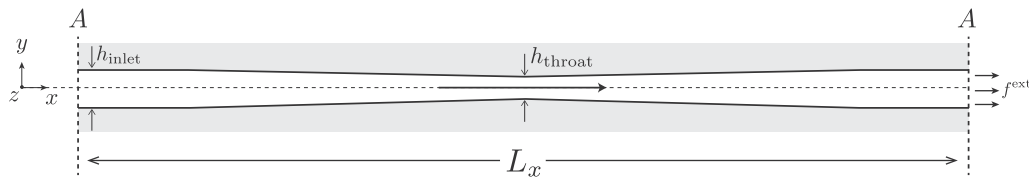


Fig. 3. Schematic (drawn to the actual proportions) of the axially-periodic converging/diverging nano-channel test case. The horizontal dotted line indicates the centre streamline, $s = x$.

3.1. Domain partitioning

For the IMM, as presented in Section 2, we subdivide the macro domain shown in Fig. 3 into parallel-flow micro elements. The height of the i th micro sub-domain is prescribed by the macro geometry, and given by:

$$h_i = h_{\text{inlet}} + (h_{\text{throat}} - h_{\text{inlet}}) \left(\frac{i-1}{\Pi-1} \right), \quad (9)$$

at streamwise positions:

$$x_i = \frac{L_x}{8} + \frac{3L_x}{8} \left(\frac{i-1}{\Pi-1} \right), \quad (10)$$

where $i = 1, 2, \dots, \Pi$. This particular domain partitioning is illustrated in Fig. 4. Note, only half of the macro domain is covered as, since we have assumed incompressible flow, the flow should be symmetrical about the throat. The ramifications of this assumption will be discussed later.

To describe the efficiency of the spatial partitioning by micro simulations, we introduce a new multiscale term: the spatial gearing, g , which quantifies the saving afforded by the multi-scale methodology in terms of the reduction in the total domain that has to be solved by a micro simulation. For this simple case:

$$g = \frac{L_x}{\Delta x \Pi}, \quad (11)$$

where Δx is the streamwise length of the individual MD sub-domains (see Fig. 5). This is the ratio of the total length of the macro domain to the sum of the micro sub-domain lengths.

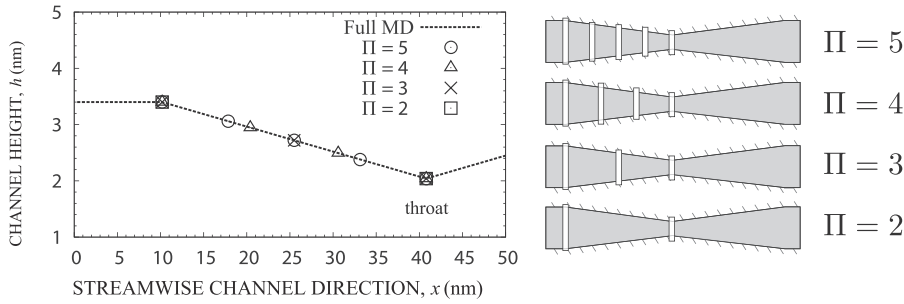


Fig. 4. Channel height variation for the full MD simulation of the converging/diverging case. Displayed also are the locations of the micro elements for $\Pi = \{2, 3, 4, 5\}$ in the converging part of the channel for the multiscale simulation.

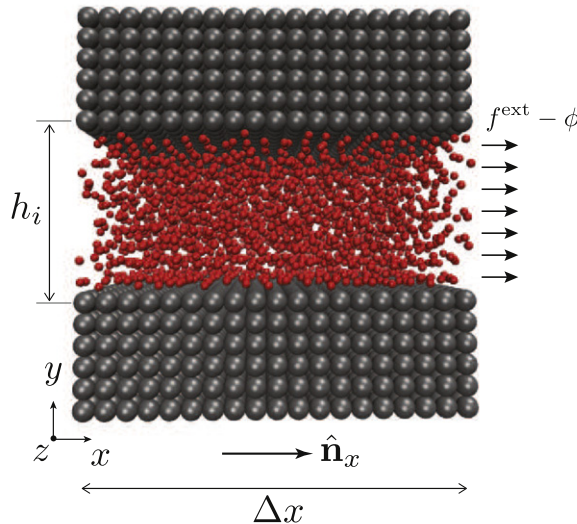


Fig. 5. MD simulation box of the i th micro sub-domain.

We can use the gearing parameter as a numerical means of adjusting the balance between computational speed-up and resolution. As g is increased, Π reduces (as Δx is likely to be fixed); this results in greater computational economy, at the expense of a poorer approximation to the quadrature in Eq. (7). Conversely, g can be reduced to improve the approximation in (7), at the expense of computational speed. In this way, gearing provides a control to balance the computational burden with solution accuracy. This is a feature of our multiscale technique (and implicitly in HMM also) that domain-decomposition hybrids do not possess. In fact, the computational cost of the latter is directly (and unavoidably) proportional to the channel length L_x , which limits the streamwise length scales of the domain that can be simulated.

3.2. The micro sub-domain solver: molecular dynamics

In this example, the micro simulations are molecular dynamics (MD) [21,22]. We use the mdFoam code [23–25], a parallelised non-equilibrium MD solver that is implemented within the OpenFOAM [26] tool box.

The streamwise (x -direction) configuration of each MD simulation sub-domain (see Fig. 5) consists of a channel with a constant cross-sectional area (as per the locally-parallel flow assumption), with the height of each given by Eq. (9). The Internal-flow Multiscale Methodology presented here enables the use of periodic boundaries in the x -direction for all micro sub-domains, which is a major convenience. The size of the box in the x -direction is chosen to be just large enough to be able to apply periodic boundary conditions without introducing spurious wrap-around effects, but still much shorter than the length of the full channel itself so as to maximise the spatial gearing (Eq. 11). The size of the micro sub-domains in the z -direction, which is also periodic, must also be large enough to avoid wrap-around effects. The sizes we choose for all micro sub-domains in the multiscale scheme here are $\Delta x = \Delta z = 6.8$ nm.

Liquid molecules at positions $\mathbf{r}_k(t) = (x_k, y_k, z_k)$, and velocities $\mathbf{v}_k(t) = (u_k, v_k, w_k)$, evolve according to Newton's equations of motion:

$$\frac{d}{dt}\mathbf{r}_k = \mathbf{v}_k(t), \quad (12)$$

$$m_k \frac{d}{dt}\mathbf{v}_k = \mathbf{f}'_k + \hat{\mathbf{n}}_x f^{\text{ext}} - \hat{\mathbf{n}}_x \phi, \quad (13)$$

where $k = (1, \dots, N)$ is a target molecule in the system, m_k is the molecule mass, f^{ext} is the external gravity-type force, and \mathbf{f}'_k is the total force due to interacting molecule neighbours:

$$\mathbf{f}'_k = \sum_{j=1(\neq k)}^N -\nabla U(r_{kj}). \quad (14)$$

The final term on the right hand side of Eq. (13) is the pressure-gradient-correction force needed to ensure macro-scale conservation of mass and momentum; as in Eq. (4), but with $\phi = \Phi/n_\rho$, where $n_\rho = \rho/m_k$ is the number density. The interaction potential $U(r_{kj})$ between liquid–liquid and wall–liquid molecules governs the physics of the flow. In this paper we simulate monatomic liquid argon using the standard 12–6 Lennard–Jones (LJ) potential:

$$U_{12-6}(r_{kj}) = \begin{cases} 4\epsilon \left[\left(\frac{\sigma}{r_{kj}} \right)^{12} - \left(\frac{\sigma}{r_{kj}} \right)^6 \right] & \text{if } r_{kj} < r_{\text{cut}}, \\ 0 & \text{if } r_{kj} \geq r_{\text{cut}}, \end{cases}$$

where $\epsilon = 1.6568 \times 10^{-21}$ J and $\sigma = 0.34 \times 10^{-9}$ m are the potential's characteristic energy and length scales, and $r_{kj} = |\mathbf{r}_k - \mathbf{r}_j|$ is the separation of two molecules (j, k) within a cut-off radius, $r_{\text{cut}} = 1.36 \times 10^{-9}$ m. The mass of each molecule is taken to be $m_k = 6.6904 \times 10^{-26}$ kg. To provide a proof-of-concept, the top and bottom walls of thickness r_{cut} are modelled using a simple cubic lattice structure at a density $\rho_w \sim 1532$ kg m $^{-3}$. The wall molecules are 'frozen' in space and time, and interact with the liquid using the same LJ parameters.

In each micro MD simulation, temperature is maintained at $T = 292.8$ K, by coupling the z -co-ordinate of molecular velocities to a Berendsen thermostat [27] with time-constant $\tau_T = 21.61$ fs. None of the MD simulations presented in this paper consider flow in the z -direction, therefore the action of the thermostat does not alter the 2D streaming velocity profiles. The liquid density $\rho_l = 1437$ kg m $^{-3}$ is set once at the beginning of all micro-simulations and remains constant (no insertions/deletions) throughout the rest of the multiscale simulation, following the assumption of flow incompressibility. The limitations of this assumption, even for low Mach number flows such as this one, will be discussed later.

3.3. IMM iterative algorithm

The solution to the multiscale problem is an iterative one, which enforces mass and momentum conservation across all the detached MD micro simulations via a pressure-gradient correction force. The algorithm stops once a convergence criterion is satisfied (based on the average mass flow rate over all micro simulations). The streamwise variation of the pressure gradient is also an output of the simulation (obtained directly from Φ_i) from which the pressure profile can be estimated. The iterative procedure is outlined in the following steps, and also illustrated in Fig. 6; n is the iteration number:

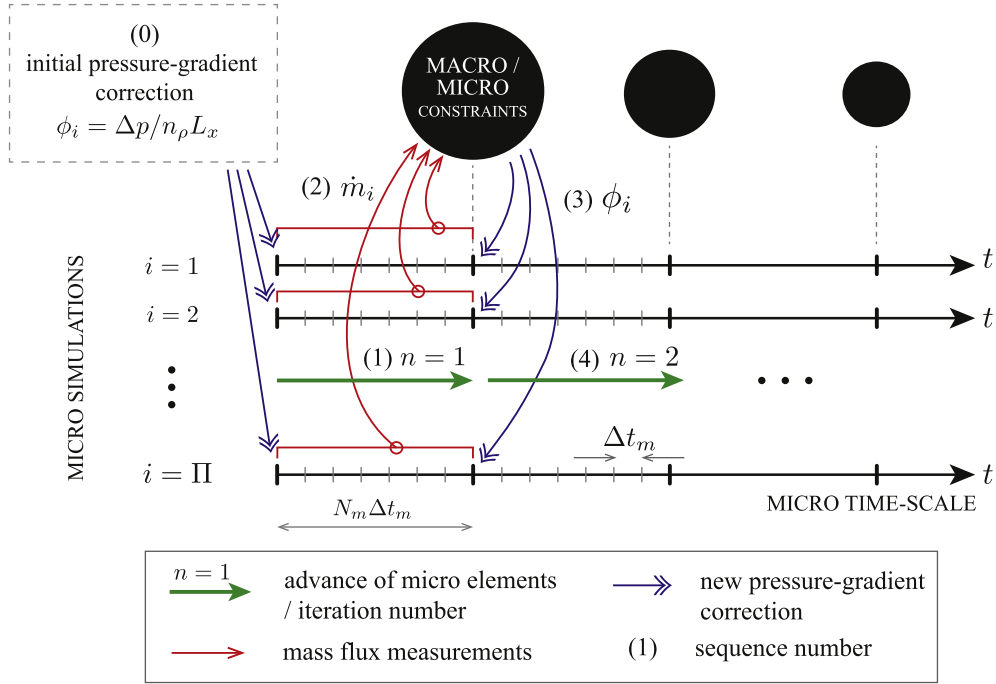


Fig. 6. Schematic depicting the IMM iterative algorithm.

- (0) Initially, set the pressure-gradient corrections in all Π micro simulations to $\phi_i^{(n=0)} = \Delta p / n_\rho L_x$. For the axially-periodic converging/diverging channel example, $\Delta p = 0$ and thus, simply: $\phi_i^{(n=0)} = 0$.
- (1) Advance all Π micro simulations for N_m molecular time-integration steps; long enough to reach steady-state and for there to be sufficient data to obtain a satisfactorily noise-free mass-flow-rate measurement.
- (2) Measure the mass flow rates \dot{m}_i (averaged over time) in each micro simulation:

$$\dot{m}_i = \frac{1}{N_m \Delta x} \sum_{t=1}^{N_m} \sum_{k=1}^{N_i} m_k \mathbf{v}_k(t) \cdot \hat{\mathbf{n}}_x, \quad (15)$$

where N_i is the number of liquid molecules in the i th MD simulation, and $m_k, \mathbf{v}_k(t)$ are each molecule's mass and instantaneous velocity, respectively.

- (3) At the new iteration step ($n+1$) compute the new pressure-gradient correction for each micro element, $\phi_i^{(n+1)}$, for the overall mass flow rate $\bar{\dot{m}}^{(n+1)}$, by solving the following set of $(\Pi+1)$ simultaneous equations:

$$\sum_{i=1}^{\Pi} a_i \phi_i^{(n+1)} = \Delta p = 0, \quad (16)$$

$$\phi_i^{(n+1)} = f^{\text{ext}} + (\phi_i^n - f^{\text{ext}}) \frac{\bar{\dot{m}}^{(n+1)}}{\dot{m}_i^{(n)}}. \quad (17)$$

These equations come directly from (7) and (8). The new pressure-gradient correction forces (a) satisfy the boundary condition on pressure drop and (b) move closer towards macroscopic mass flux conservation.

- (4) Repeat from (1) until convergence. As a convergence criterion, we take: $|(\bar{\dot{m}}^n - \bar{\dot{m}}^{n-1}) / \bar{\dot{m}}^n| < \zeta_{\text{tol}}$, where ζ_{tol} is a user-set tolerance.

4. Results: comparison with a full MD simulation

In this paper we use a full MD solution of the axially-periodic converging/diverging channel configuration (Fig. 3) as a means to validate results from our multiscale procedure; as such, we consider a full MD approach as the 'accurate' solution of the case. The MD case setup is shown in Fig. 7. The same description of the walls used in the micro simulations is used, with the exception that, in the full case there is channel-height variation in the streamwise direction. All other conditions are the same, including the external force f^{ext} , initial number density and the Berendsen thermostat parameters. One measurement plane is placed at the throat (as shown in Fig. 7) to compute the mean mass flux through the channel for comparison

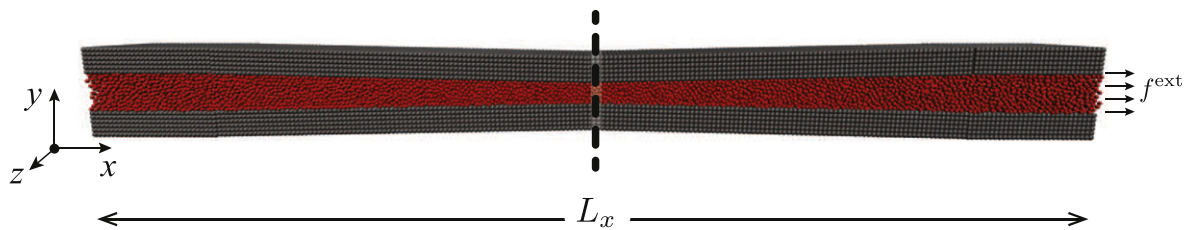


Fig. 7. Simulation setup for full MD solution of the converging/diverging nanochannel case. The vertical dotted line located at the throat of the channel represents the mass-flux measurement plane.

with the multiscale prediction. The net mass flow rate at a plane is measured by averaging the number of molecules that cross it in a prescribed time period; molecules which cross in the positive x -direction are counted as positive and those which cross in the opposite direction are counted as negative.

4.1. IMM results

We consider four cases of the domain partitioning of the channel geometry: $\Pi = \{2, 3, 4, 5\}$. The micro simulations in each case are uniformly distributed in the streamwise direction on the converging side of the channel; see Fig. 4. These cases correspond to the gears $g = \{6, 4, 3, 2, 4\}$, respectively. As mentioned earlier, this case is symmetric so that the results on one side of the throat can be mapped onto the other.

The IMM results for the micro sub-domain mass flow rates (\dot{m}_i) and total forces ($f^{\text{ext}} - \phi_i$) from each case are shown in Figs. 8 and 9, respectively. The convergence characteristics are shown in Fig. 10. What is evident in all cases is a very quick convergence of the multiscale simulations, occurring after roughly two iterations. This is a positive and attractive outcome of our approach when compared to domain-decomposition techniques that generally take 10–20 iterations to converge to steady-state [14]. Furthermore, and in contrast to domain-decomposition, we found no need for iteration-relaxation to

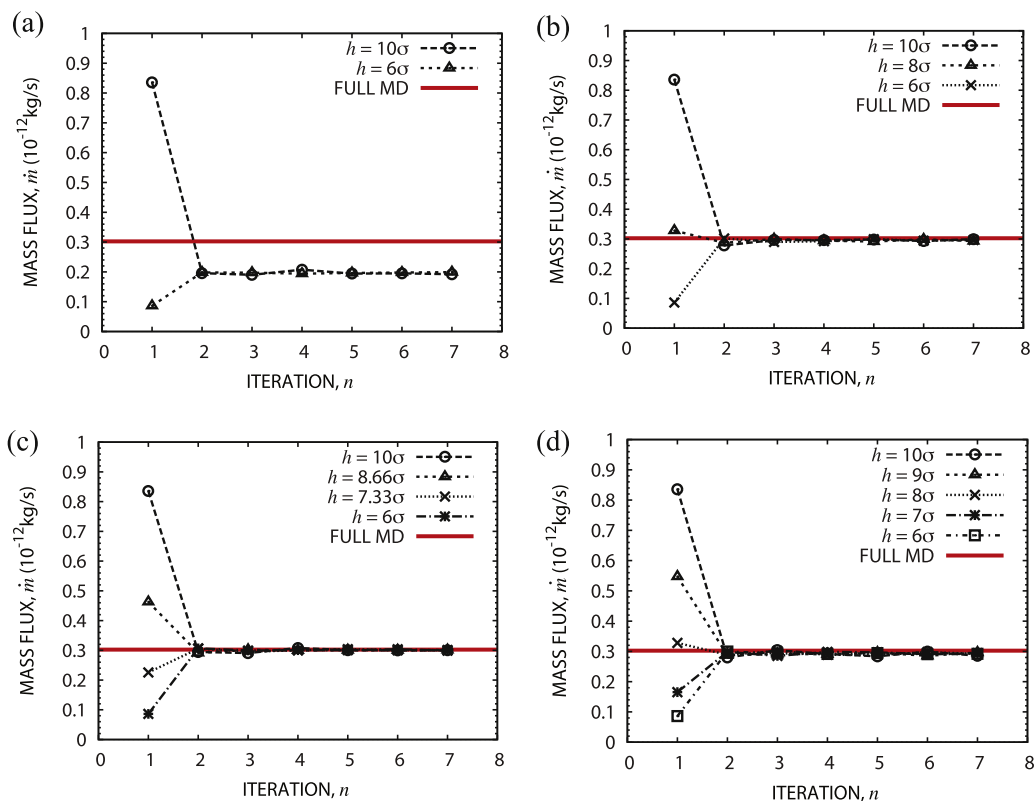


Fig. 8. Convergence of the individual micro mass fluxes at progressive iterations (n) of the multiscale scheme for various number of micro elements per multiscale simulation: (a) $\Pi = 2$, (b) $\Pi = 3$, (c) $\Pi = 4$, and (d) $\Pi = 5$. Each iteration corresponds to $\tau_m = 800,000$ MD time-steps. Error bars are smaller than the sizes of the symbols and have been omitted from the graphs.

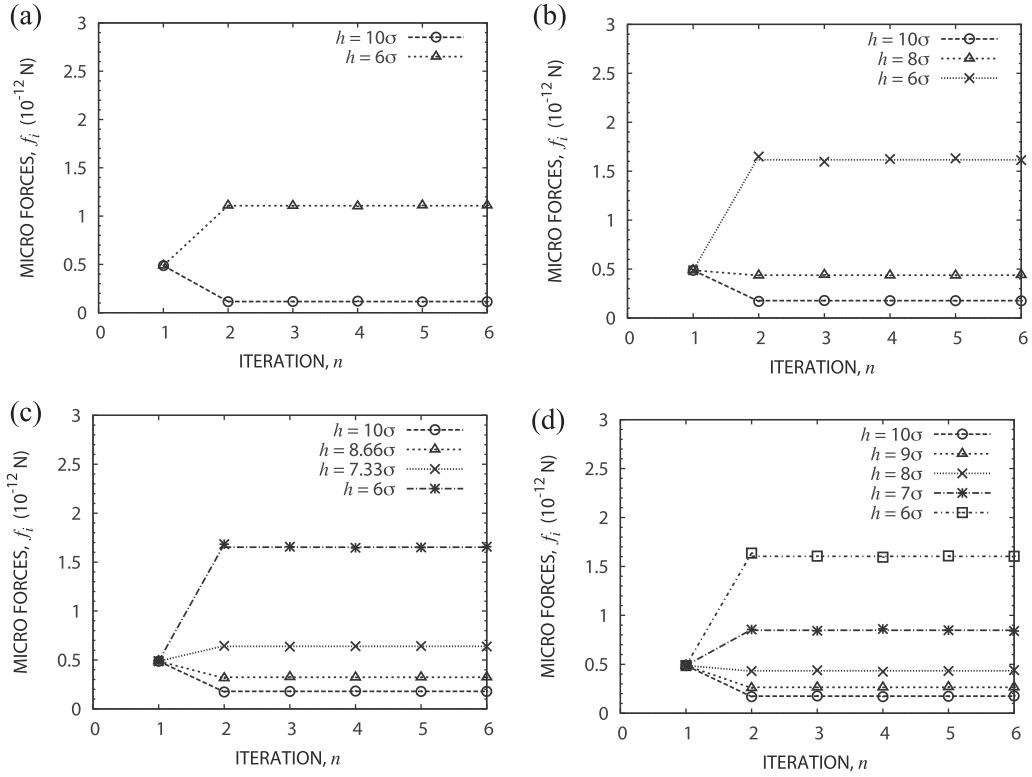


Fig. 9. Micro forces $f_i = f_i^{\text{ext}} - \phi_i$ at progressive iterations (n) for various number of micro elements per multiscale simulation: (a) $\Pi = 2$, (b) $\Pi = 3$, (c) $\Pi = 4$, and (d) $\Pi = 5$. Convergence is quick, occurring after $n = 2$ iterations.

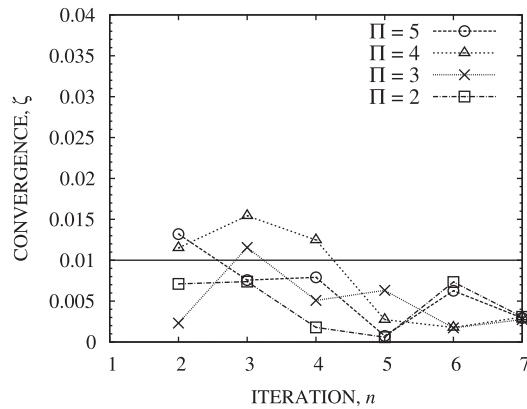


Fig. 10. Convergence of consecutive average mass fluxes, $\zeta = |(\bar{m}^{(n)} - \bar{m}^{(n-1)})/\bar{m}^{(n)}|$ at progressive iterations (n). The horizontal line is the chosen tolerance fraction, $\zeta_{\text{tol}} = 0.01$.

smooth the transition to micro/macro convergence. The order of fluctuations present in the convergence measurements (Fig. 10) is expected since there is a standard error of the mean of $\pm 0.008 \times 10^{-12}$ kg/s in the measured micro element mass fluxes.

For the purposes of validation, we plot the mass flow rate obtained from the full MD simulation on all graphs in Fig. 8. For each multi-scale case ($\Pi = \{2, 3, 4, 5\}$) the percentage difference in the mass flow rates (MD and multiscale) is calculated and plotted in Fig. 11. As is perhaps to be expected, the case that is discretized with $\Pi=2$ micro elements, which barely represents the geometry of the channel, is in error by 35% from the full MD result. Very reassuringly, though, for $\Pi > 2$ the error reduces to a consistently low level, of the order of 1–3%. For this particular flow case, it would seem that even as few as $\Pi = 3$ micro sub-domains are sufficient to obtain a satisfactory agreement with the full MD simulation, corresponding to a gearing of $g = 4$.

In Fig. 12 we present the streamwise distribution of the pressure-gradient correction, $\Phi_i = \phi_i n_p (= dp/dx|_i)$ for the three cases $\Pi = \{3, 4, 5\}$. As was observed with the mass flow rate, the method quickly converges with increasing Π ; we can

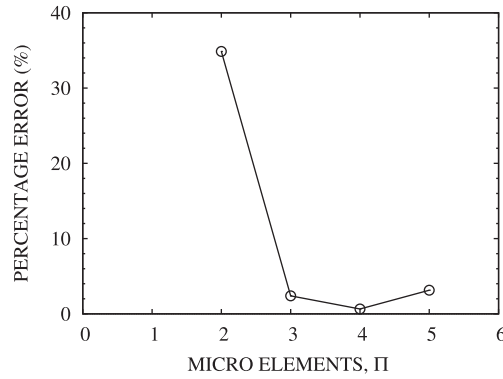


Fig. 11. Comparisons of mass flux computed from the multiscale simulations (\bar{m}) with results measured from the full MD run (\dot{m}_F). The percentage error is calculated using $(\dot{m}_F - \bar{m})/\dot{m}_F \times 100$.

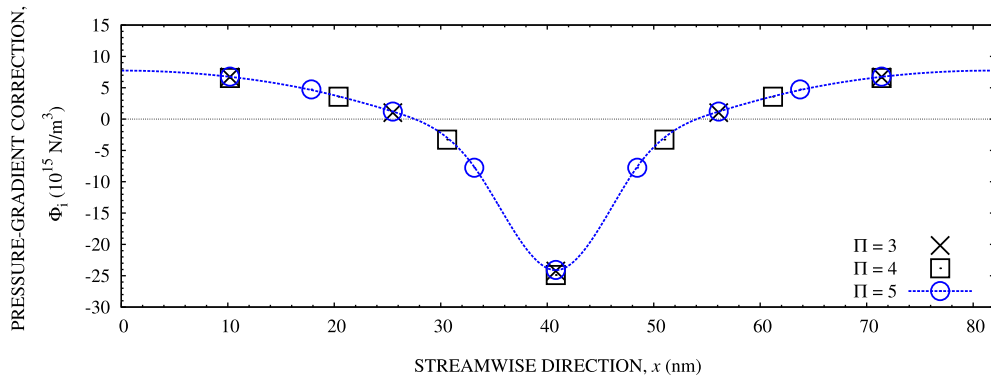


Fig. 12. Pressure-gradient correction for different cases $\Pi = \{3, 4, 5\}$. For case $\Pi = 5$ a spline is fitted through the data points.

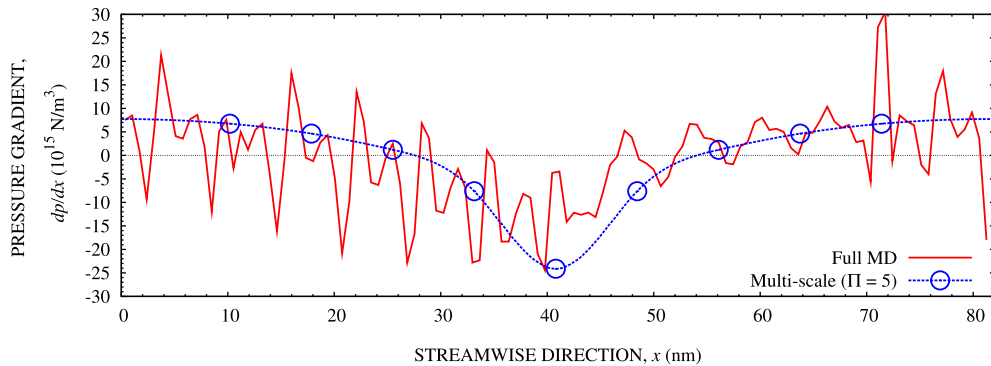


Fig. 13. Pressure-gradient correction for case $\Pi = 5$; comparison with full MD.

conclude that $\Pi = 5$ is more than sufficient for this particular geometry. In Fig. 13, this most accurate case ($\Pi = 5$) is compared to the pressure gradient calculated directly from the full MD simulation, using the Irving–Kirkwood equation for pressure [28] evaluated in small streamwise bins. The streamwise pressure profile from the multiscale simulation can be reconstructed from Φ_i by numerical integration over x and adding the absolute mean value of pressure (obtained from an Irving–Kirkwood measurement across all micro elements). This is also compared to the pressure calculated directly from the full MD simulation in Fig. 14. Note, our multiscale approach could be an alternative method for computing pressure variations in non-equilibrium MD simulations of nano-channels.

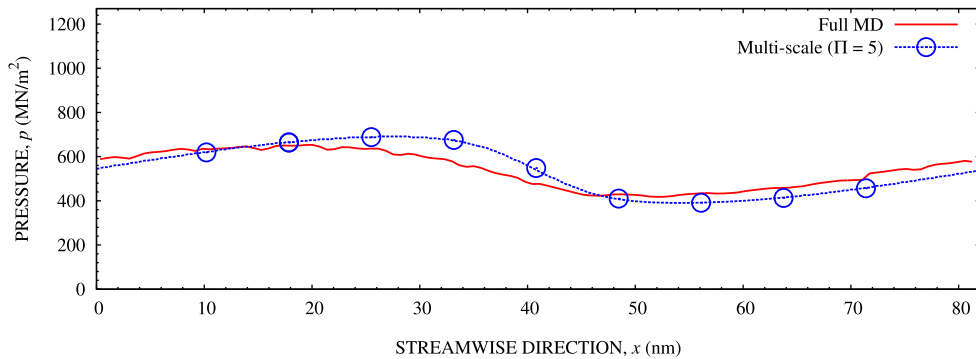


Fig. 14. Streamwise distribution of pressure for case $\Pi = 5$; comparison with full MD.

4.2. Sources of error

The results presented in Figs. 8–11 demonstrate that the multiscale method presented in this paper works well. Provided there are sufficient micro subdomains, the mass-flow-rate measurements are within 1–3% of the predictions from a full MD simulation of the geometry. The multiscale prediction of streamwise variation of pressure gradient and pressure (in Figs. 13 and 14) are acceptable, but less good. There are numerical, statistical and physical approximations inherent in the method, and these are considered in turn as potential sources of error.

The numerical approximation of this method lies in the quadrature in Eq. (7). We have shown in Figs. 11 and 12 that for $\Pi = 5$ the results are converged to a satisfactory level, and therefore we can discount lack of resolution in the micro subdomains as being the source of any discrepancy in this case. The discrepancy is not, either, a matter of statistical fluctuations in mass-flux measurements, which is kept to an acceptable level for these simulations. The physical approximations of subsonic, low-speed, locally-parallel flow, used in the formulation presented in Section 2, are also all safe given $Ma = 0.015$, $Re = 0.8$ and $S = 22.5$.

What is not entirely safe to assume, however, is incompressibility, despite the low Mach number. Arguments presented in [29] explain why, even at low Mach numbers, significant compressibility can occur in micro and nano geometries. The head loss due to viscous forces in our nano channel case is large, and over long channel length scales the pressure change becomes a non-negligible proportion of the mean pressure; this is why, at constant temperature, compressibility could be significant. To investigate this, we plot in Fig. 15 the streamwise density variation extracted from the full MD simulation. It can be seen that the maximum density value is almost 14% greater than the minimum value. Ignoring this variation will have had some, although not serious, impact on the multiscale results, since proportionally more mass flux is generated, for the same pressure gradient, in a high density region as compared to a low density region. This is most likely the cause of the discrepancies between the multiscale results and the full MD that are seen in Figs. 13 and 14. Interestingly, the mass-flow-rate predictions of the IMM appear to be not that susceptible to the omission of the density variation. This is probably because the influence of the low and high regions of density counteract each other in determining the global mass flow rate, but are in evidence when plotting streamwise variation of the pressure, for example.

It is important to note that the assumption of incompressibility is not inherent in the general IMM presented in Section 2. What is required is the ability to (a) calculate density variations from pressure profiles (as constructed in Fig. 14) and (b) set values of density in individual micro sub domains. This extension of the method will be the subject of further work.

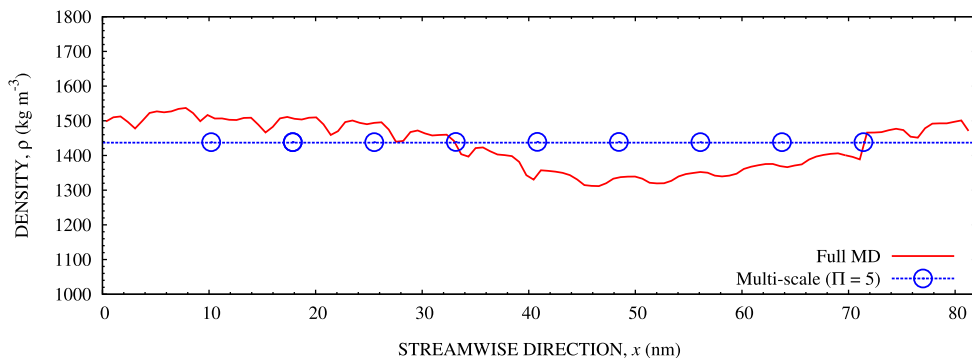


Fig. 15. Fluid density calculated from the full MD simulation compared with the multiscale simulation with $\Pi = 5$.

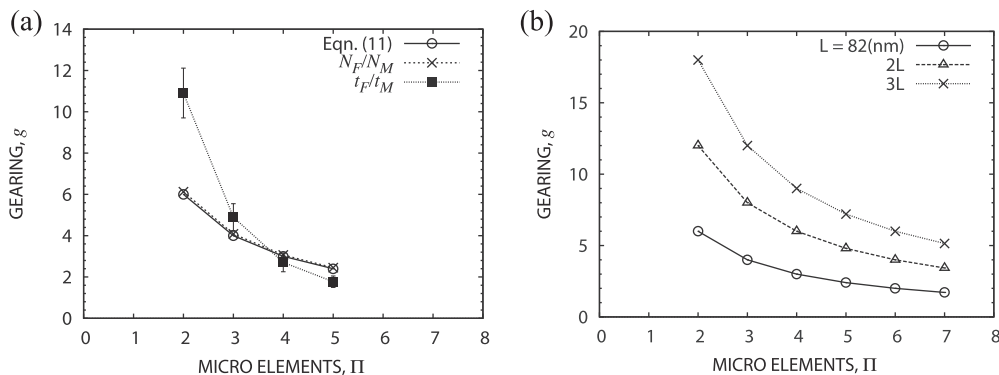


Fig. 16. (a) Computational speed-up for the multiscale method and (b) gearing characteristics for longer converging/diverging channels.

4.3. Computational speed-up

The gearing parameter g , defined in Eq. (11), provides an indication of the computational speed-up of our multi-scale method as compared to a pure MD simulation of the same case. In Fig. 16(a) we show that g from Eq. (11) is almost identical to a gearing parameter formulated by explicitly comparing the number of molecules in the full and the multiscale simulations ($= N_F/N_M = N_F/\sum_i^{\Pi} N_i$). Furthermore, Fig. 16(a) plots also a gearing computed from the clock-times of each simulation ($= t_F/t_M$). To make a fair comparison, the total computational times measured from separate simulations (t_F, t_M) were both normalised by the processing power assigned to it. For example, Π processors are assigned to each multiscale simulation (one micro element per processor); the total time of the multiscale simulation is then $t_M = \sum_i^{\Pi} t_i \Pi$, where t_i is the total measured time for the i th micro element to converge to steady-state (~ 3 iterations). The full MD simulation was run on 24 processors, and so the total time of the simulation to reach steady-state and gather statistics (2.4 million MD time-steps) was multiplied by 24.

Two promising features of our multiscale method are seen in Fig. 16(b), which shows projected values of the gearing parameter for various lengths of the converging/diverging channel flow problem. Each point on the graph represents a different multiscale configuration for a particular geometry. Unlike a full MD simulation, which has little flexibility in the amount of processing power required to solve a particular problem, the IMM approach enables direct adjustment of the balance between accuracy and resolution to suit the computational resources available. Also, greater computational savings are expected for longer channel lengths because the scale separation will increase in proportion to the length of the channel, allowing the same number of micro elements to be used without any penalty in accuracy. Therefore, for modelling much higher aspect ratio flow systems than that considered in this paper, for which a full MD approach is computationally intractable, our multiscale technique is a viable and practical alternative.

5. Conclusions

While domain-decomposition methods are currently the most popular hybrid approach to reducing the computational effort of a full molecular calculation, there are still some problems associated with this formulation. For example, the unavoidable issue of length- and time-scale decoupling, as well as the complexity of coupling physical properties at non-periodic MD interfaces.

In this paper we have proposed an alternative: a new micro-resolution multiscale method that addresses these issues for high-aspect-ratio micro/nanoflows. This method has been demonstrated on an axially-periodic converging/diverging nanochannel flow driven by a gravity-type body force. For this internal flow problem, the channel was partitioned uniformly into isolated micro elements along the streamwise direction, each having a height corresponding to the local converging/diverging geometry. The concept of gearing has been introduced, which permits a compromise between computational speed-up and resolution. This is an attractive feature of our method, not possible in domain-decomposition methods. Domain-decomposition methods in any case struggle with very extended micro/nano flows, as the MD sub-domains need to cover the entire streamwise length of the geometry.

Our novel macro/micro coupling technique maintains the simplicity of periodicity in all the micro simulations, and works on pressure-gradient (rather than velocity or strain-rate) corrections derived from *global* constraints of the mass and momentum fluxes. This coupling approach does not require the complicated exchange of stresses/strains (for constitutive relation correction) or velocity slip values (for boundary correction), as are required in the HMM approach. Instead, all that is required from the micro elements of our method are mass fluxes; all that is required from the macro solver are body forces that are then prescribed in each micro element. The algorithm converges remarkably well after a few iterations to the same mass flow rate that is calculated from a full MD simulation of the same case.

The computational savings of the demonstration case in this paper are modest, due our requirement to validate the scheme with an accurate and full MD simulation. The true potential of our new method emerges for much longer (and more realistic) scale-separated flows ($S \gg 1$) and for high gearings ($g \gg 1$); that is, longer channels/tubes and more widely-spaced micro subdomains.

While the method has been demonstrated here on a flow bounded by solid surfaces, it could equally be applied to surface or interface flows of high aspect ratio (in the streamwise direction)—such as very thin coating flows—provided that the upper (in the case of coating flows, free surface) boundary conditions are properly represented in both the macro and micro solvers. This will be the subject of future work.

Acknowledgements

This work is financially supported in the UK by EPSRC Programme Grant EP/I011927/1. The authors thank the reviewers of this paper for their very helpful comments.

References

- [1] W.D. Nicholls, M.K. Borg, D.A. Lockerby, J.M. Reese, Water transport through (7,7) carbon nanotubes of different lengths using molecular dynamics, *Microfluidics and Nanofluidics* 12 (2012) 257–264.
- [2] D. Mantzalis, N. Asproulis, D. Drikakis, Filtering carbon dioxide through carbon nanotubes, *Chemical Physics Letters* 506 (2011) 81–85.
- [3] S.-J. Heo, S.B. Sinnott, D.W. Brenner, J.A. Harrison, Computational modeling of nanometer-scale tribology, in: B. Bhushan (Ed.), *Nanotribology and Nanomechanics*, Springer, Berlin Heidelberg, 2005, pp. 623–691.
- [4] H.S. Wijesinghe, N.G. Hadjiconstantinou, Discussion of hybrid atomistic-continuum methods for multiscale hydrodynamics, *International Journal of Multiscale Computational Engineering* (2004) 189–202.
- [5] K. Mohamed, A. Mohamad, A review of the development of hybrid atomistic-continuum methods for dense fluids, *Microfluidics and Nanofluidics* 8 (2010) 283–302.
- [6] H. Okumura, D.M. Heyes, Comparisons between molecular dynamics and hydrodynamics treatment of nonstationary thermal processes in a liquid, *Physical Review E* 70 (2004) 061206.
- [7] S.T. O'Connell, P.A. Thompson, Molecular dynamics–continuum hybrid computations: a tool for studying complex fluid flows, *Physical Review E* 52 (1995) R5792–R5795.
- [8] N. Hadjiconstantinou, A. Patera, Heterogeneous atomistic-continuum methods for dense fluid systems, *International Journal of Modern Physics C* 8 (1997) 967–976.
- [9] R. Delgado-Buscalioni, P.V. Coveney, Continuum-particle hybrid coupling for mass, momentum, and energy transfers in unsteady fluid flow, *Physical Review E* 67 (2003) 1–13.
- [10] W. Ren, W.E., Heterogeneous multiscale method for the modeling of complex fluids and micro-fluidics, *Journal of Computational Physics* 204 (2005) 1–26.
- [11] S. Yasuda, R. Yamamoto, A model for hybrid simulations of molecular dynamics and computational fluid dynamics, *Physics of Fluids* 20 (2008) 113101.
- [12] N. Asproulis, M. Kalweit, D. Drikakis, A hybrid molecular continuum method using point wise coupling, *Advances in Engineering Software* 46 (2012) 85–92.
- [13] X.B. Nie, S.Y. Chen, W. E, M.O. Robbins, A continuum and molecular dynamics hybrid method for micro- and nano-fluid flow, *Journal of Fluid Mechanics* 500 (2004) 55–64.
- [14] T. Werder, J.H. Walther, P. Koumoutsakos, Hybrid atomistic-continuum method for the simulation of dense fluid flows, *Journal of Computational Physics* 205 (2005) 373–390.
- [15] E.G. Flekky, G. Wagner, J. Feder, Hybrid model for combined particle and continuum dynamics, *Europhysics Letters* 52 (2000) 271–276.
- [16] E.G. Flekky, R. Delgado-Buscalioni, P.V. Coveney, Flux boundary conditions in particle simulations, *Physical Review E (Statistical, Nonlinear, and Soft Matter Physics)* 72 (2005) 026703.
- [17] R. Delgado-Buscalioni, P.V. Coveney, Hybrid molecular-continuum fluid dynamics, *Philosophical Transactions of the Royal Society London A* 362 (2004) 1639–1654.
- [18] R. Delgado-Buscalioni, E.G. Flekky, P.V. Coveney, Fluctuations and continuity in particle-continuum hybrid simulations of unsteady flows based on flux-exchange, *Europhysics Letters* 69 (2005) 959–965.
- [19] W. E, W. Ren, E. Vanden-Eijnden, A general strategy for designing seamless multiscale methods, *Journal of Computational Physics* 228 (2009) 5437–5453.
- [20] A.W. Lees, S.F. Edwards, The computer study of transport processes under extreme conditions, *Journal of Physics C (Solid State Physics)* 5 (1972) 1921–1928.
- [21] M.P. Allen, D.J. Tildesley, *Computer Simulation of Liquids*, Oxford University Press, 1987.
- [22] D.C. Rapaport, *The Art of Molecular Dynamics Simulation*, second ed., Cambridge University Press, 2004.
- [23] G.B. Macpherson, M.K. Borg, J.M. Reese, Generation of initial molecular dynamics configurations in arbitrary geometries and in parallel, *Molecular Simulation* 33 (2007) 1199–1212.
- [24] G.B. Macpherson, J.M. Reese, Molecular dynamics in arbitrary geometries: Parallel evaluation of pair forces, *Molecular Simulation* 34 (2008) 97–115.
- [25] M.K. Borg, G.B. Macpherson, J.M. Reese, Controllers for imposing continuum-to-molecular boundary conditions in arbitrary fluid flow geometries, *Molecular Simulation* 36 (2010) 745.
- [26] OpenFOAM. <www.openfoam.org>, 2012 (last accessed October).
- [27] H.J.C. Berendsen, J.P.M. Postma, W.F. van Gunsteren, A. Dinola, J.R. Haak, Molecular dynamics with coupling to an external bath, *Journal of Chemical Physics* 81 (1984) 3684–3690.
- [28] J.H. Irving, J.G. Kirkwood, The statistical mechanical theory of transport processes. IV. The equations of hydrodynamics, *Journal of Chemical Physics* 18 (1950) 817–829.
- [29] M. Gad-El-Hak, *MEMS [electronic resource]: Introduction and Fundamentals*, second ed., CRC Taylor and Francis, 2006.